Journal of Geophysical Research: Atmospheres

Supporting Information for

Energy Budget Constraints on the Time History of Aerosol Forcing and Climate Sensitivity

C. J. Smith[1,2], G. R. Harris[3], M. D. Palmer[3], N. Bellouin[4], W. Collins[4], G. Myhre[5], M. Schulz[6], J.-C. Golaz[7], M. Ringer[3], T. Storelvmo[8] and P. M. Forster[1]

[1]Priestley International Centre for Climate, University of Leeds, UK. [2]International Institute for Applied Systems Analysis (IIASA), Laxenburg, Austria. [3]Met Office Hadley Centre, Exeter, UK. [4]Department of Meteorology, University of Reading, UK. [5]Center for International Climate and Environmental Research in Oslo (CICERO), Norway. [6]Norwegian Meteorological Institute, Oslo, Norway. [7]Lawrence Livermore National Laboratory, Livermore, CA, USA. [8]Department of Geosciences, University of Oslo, Norway.

Contents of this file

Text S1. Non-aerosol radiative forcing timeseries

This supplementary text describes the non-aerosol forcing time series used in the simulations. Most forcing categories are similar to those used in version 1.3 of the Finite-amplitude Impulse Response model (FaIR; Smith, Forster, et al., 2018) with updates where appropriate. Where uncertainty ranges are given, they are taken to be 90% confidence intervals on the 1750-2019 forcing.

Greenhouse gases

Greenhouse gas (GHG) forcings are calculated from concentration to radiative forcing (RF) relationships (Etminan et al., 2016; Hodnebrog, Aamaas, et al., 2020). The re-fitting of the original Oslo line-by-line radiative transfer model results for RF from CO_2, CH_4 and N_2O (Etminan et al., 2016) as implemented by Meinshausen et al. (2020) are used, which reduces the relative error in the fits. GHG concentrations are taken from the observationally-based CMIP6 historical time series for 1750-2014 (Meinshausen et al., 2017) extended forwards to 2020 using the SSP2-4.5 pathway (Gidden et al., 2019). To move from RF to ERF, 5% is added to the RF for CO_2 and 14% subtracted from CH_4 to account for land-surface warming and tropospheric adjustments respectively (Smith, Kramer, et al., 2018). Tropospheric adjustments also account for an additional 7% for N_2O, 13% for CFC-11 and 12% for CFC-12 (Hodnebrog, Myhre, et al., 2020). For all

other GHGs, ERF is assumed to be the same as RF. We apply a ±20% relative uncertainty (5-95% range) on the present-day ERF from CO_2, N_2O and other GHGs except CH_4 for which we apply ±28%; this follows AR5 (Myhre et al., 2013b) with an increase in the uncertainty for CH_4 following Etminan et al. (2016). CMIP6 model results suggest these ranges are conservative and the ERF spread is possibly lower (Smith et al., 2020). We do not modify the shape of the historical greenhouse gas forcing as historical concentrations are known with low uncertainty.

Ozone

Historical tropospheric and stratospheric ozone forcing is used from the subset of CMIP6 models in Skeie et al. (2020) that (i) include full tropospheric chemistry; (ii) are not too structurally similar to other models and (iii) produce sensible pre-industrial to present-day ozone forcing estimates (hence UKESM1-0-LL is excluded due to its implausible negative present-day forcing). The full list of retained models from Skeie et al. (2020) is BCC-ESM1-0, CESM2(WACCM6), GFDL-ESM4, GISS-E2-1-H, MRI-ESM2-0 and Oslo-CTM3. For extrapolating tropospheric ozone ERF back before 1850 and forward after 2014, we use CMIP6 historical and SSP2-4.5 precursor emissions to forcing relationships for CO, NOx, non-methane volatile organic compounds and concentrations of CH_4 from Smith, Forster, et al. (2018), based on Stevenson et al. (2013), and re-fit these coefficients to correspond to the CMIP6 emissions and Skeie et al. (2020) forcing. We use a ±50% uncertainty on the best estimate of tropospheric ozone ERF of +0.41 W m^{-2} for 1750-2019. Stratospheric ozone forcing follows the same method, for which the Skeie et al. (2020) model results show that stratospheric ozone depletion from halogenated gases is outweighed by ozone formation from short-lived climate forcers. Stratospheric ozone has a best estimate 1750-2019 ERF of +0.07 W m^{-2} to which we apply a ±200% relative uncertainty.

Other anthropogenic forcings

Land use forcing of -0.20 W m^{-2} from 1750-2019 is used as our best estimate, using land-use-derived albedo change from Ghimire et al. (2014) of -0.15 W m^{-2} with irrigation effects on formation of low-level clouds assumed to contribute an additional -0.05 W m^{-2} (Sherwood et al., 2018). To this total land-use forcing we apply a ±75% relative uncertainty. For aviation contrail and contrail-induced cirrus forcing, we use the recent comprehensive assessment of Lee et al. (2020) of 0.0574 (0.019 to 0.098) W m^{-2} for 1750-2018, and extrapolated this forward one year using aviation NOx projections from SSP2-4.5. Black carbon on snow forcing follows BC emissions in the SSP-historical and SSP2-4.5 time series and is scaled to 0.08 W m^{-2} in 2019 relative to 1750, which is the AR5 best estimate doubled to take into account the forcing efficacy of black carbon on snow assessed as being greater than unity (Bond et al., 2013). The lognormal distribution for the uncertainty range of 0.04 to 0.18 W m^{-2} is applied following AR5 (Myhre et al., 2013a). Stratospheric water vapor from methane oxidation is assumed to have a 1750-2019 best estimate forcing of 0.05 W m^{-2} with a ±100% relative uncertainty.

Volcanic forcing

Volcanic ERF is calculated using -20τ from CMIP5 models (Larson & Portmann, 2016) and an analysis of seven CMIP6 models that provided the piClim-histnat (natural forcings

only) experiment (Fig. S8), where τ is the stratospheric aerosol optical depth (SAOD) at 550 nm. From the CMIP6 models, an estimate of the solar forcing (see below) was subtracted from the total natural forcing to estimate the volcanic forcing. We combine 3 overlapping datasets for SAOD: the eVolv database for the period 500 BCE to 1900 CE (Toohey & Sigl, 2017), the CMIP6 historical volcanic SAOD for 1850-2014, and the GloSSAC dataset for 1979-2018 (Kovilakam et al., 2020). The GloSSAC dataset is converted from SAOD at 525 nm to the target 550 nm using an Ångstrom exponent of -2.33 (Kovilakam et al., 2020). For 2019 we repeat 2018 noting no significant eruptions occurred (Global Volcanism Program, 2013). A linear transition between eVolv and CMIP6 is performed for 1850-1900 and for CMIP6 to GloSSAC for 1979-1989. The time-mean SAOD over the 2519 years of available data is defined to be the zero forcing, such that quiescent years have a small positive forcing. The rationale for this is that the long-term mean temperature anomaly should be zero when only volcanic forcing is present. Following AR5 analysis of recent eruptions, volcanic ERF is given an uncertainty range of ±50%.

Solar forcing

The solar forcing is taken from the derived SATIRE-M ^{14}C solar irradiance database for the 9000 years up to 2014 (Vieira et al., 2011) and the concurrent CMIP6 total solar irradiance from 2015 onwards (Matthes et al., 2017). The solar irradiance timeseries is referenced to the two solar cycles spanning 1745-1765, as a proxy for 1750 conditions. Effective radiative forcing from solar variability is then calculated from the annual total solar irradiance anomaly, multiplied by ¼ (geometric effect) × 0.71 (planetary co-albedo) × 0.72 (tropospheric and stratospheric adjustments (Gray et al., 2009; Smith, Kramer, et al., 2018)). To project uncertainty in the solar forcing time series, we vary both the amplitude of the solar magnitude fluctuations (±50%) and the overall solar forcing trend from 1750 to 2019 (0.0 ± 0.1 W m^{-2} as a linear trend).

.

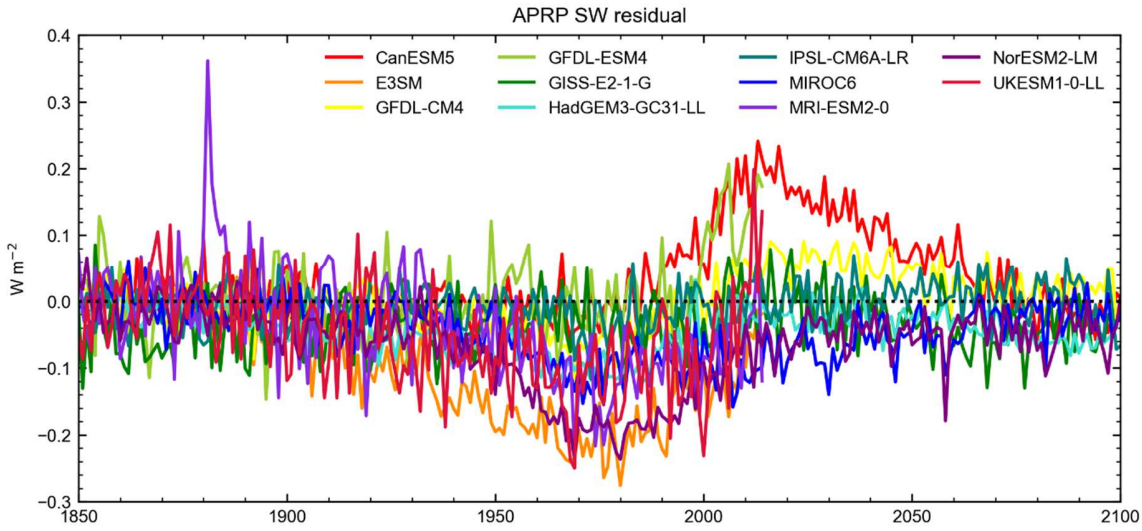

Figure S1: Residual from shortwave APRP decomposition of aerosol ERF in RFMIP and AerChemMIP models and E3SM (showing ERF_{SW} - $ERFari_{SW}$ - $ERFaci_{SW}$)

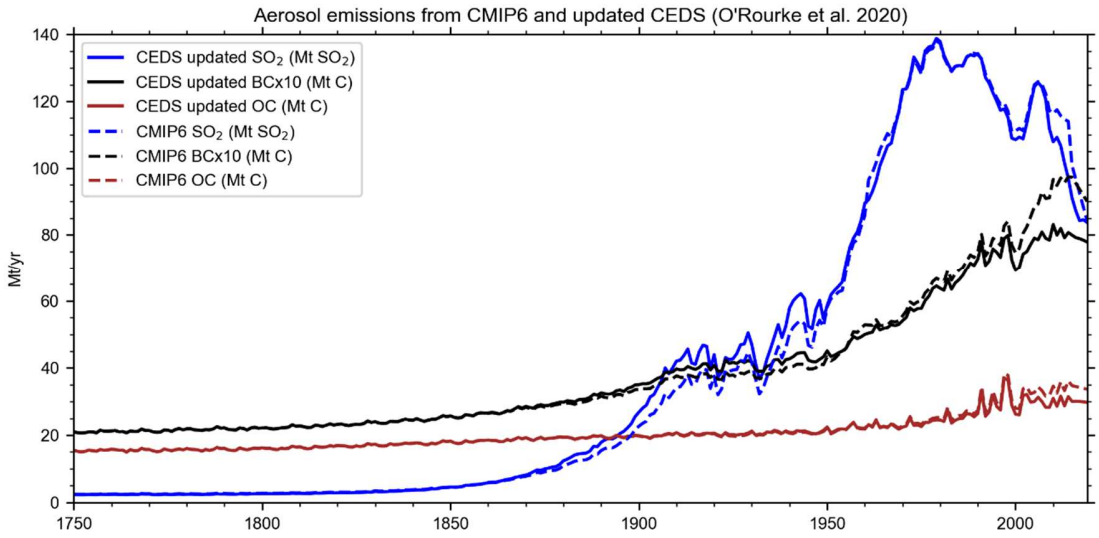

Figure S2: Comparison of the CMIP6 emissions dataset (dashed lines), used in running the CMIP6 models, with the updated CEDS emissions (O'Rourke et al., 2020) plus biomass burning emissions which are unchanged (solid lines) used for generating the CMIP6-constrained forcing time series.

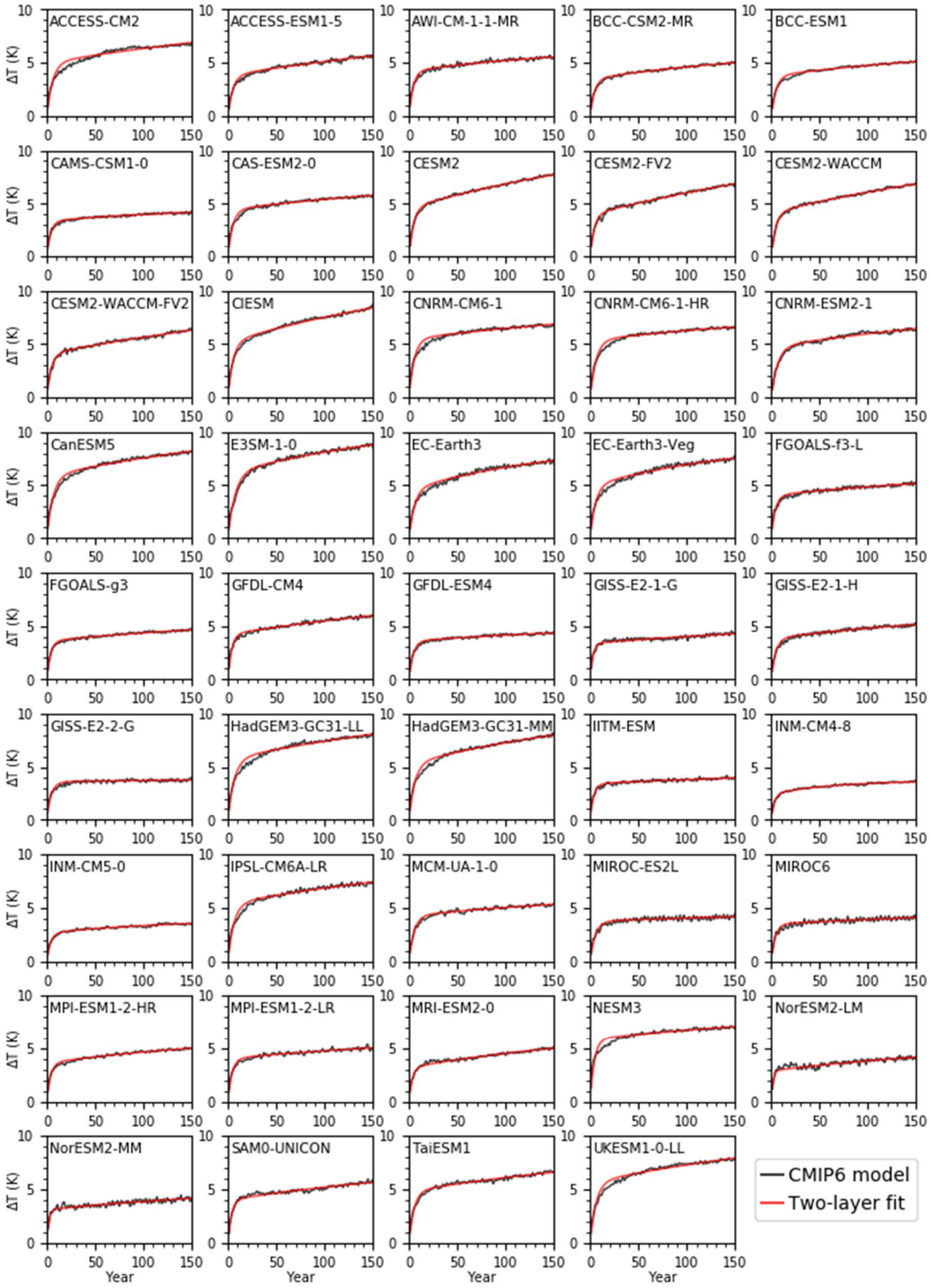
ACCESS-CM2
ACCESS-ESM1-5
AWI-CM-1-1-MR
BCC-CSM2-MR
BCC-ESM1
CAMS-CSM1-0
CAS-ESM2-0
CESM2
CESM2-FV2
CESM2-WACCM
CESM2-WACCM-FV2
CIESM
CNRM-CM6-1
CNRM-CM6-1-HR
CNRM-ESM2-1
CanESM5
E3SM-1-0
EC-Earth3
EC-Earth3-Veg
FGOALS-f3-L
FGOALS-g3
GFDL-CM4
GFDL-ESM4
GISS-E2-1-G
GISS-E2-1-H
GISS-E2-2-G
HadGEM3-GC31-LL
HadGEM3-GC31-MM
IITM-ESM
INM-CM4-8
INM-CM5-0
IPSL-CM6A-LR
MCM-UA-1-0
MIROC-ES2L
MIROC6
MPI-ESM1-2-HR
MPI-ESM1-2-LR
MRI-ESM2-0
NESM3
NorESM2-LM
NorESM2-MM
SAM0-UNICON
TaiESM1
UKESM1-0-LL
ΔT (K)
Year
CMIP6 model
Two-layer fit

Figure S3: Two-layer model fits to CMIP6 abrupt 4xCO_2 global surface air temperature (GSAT).

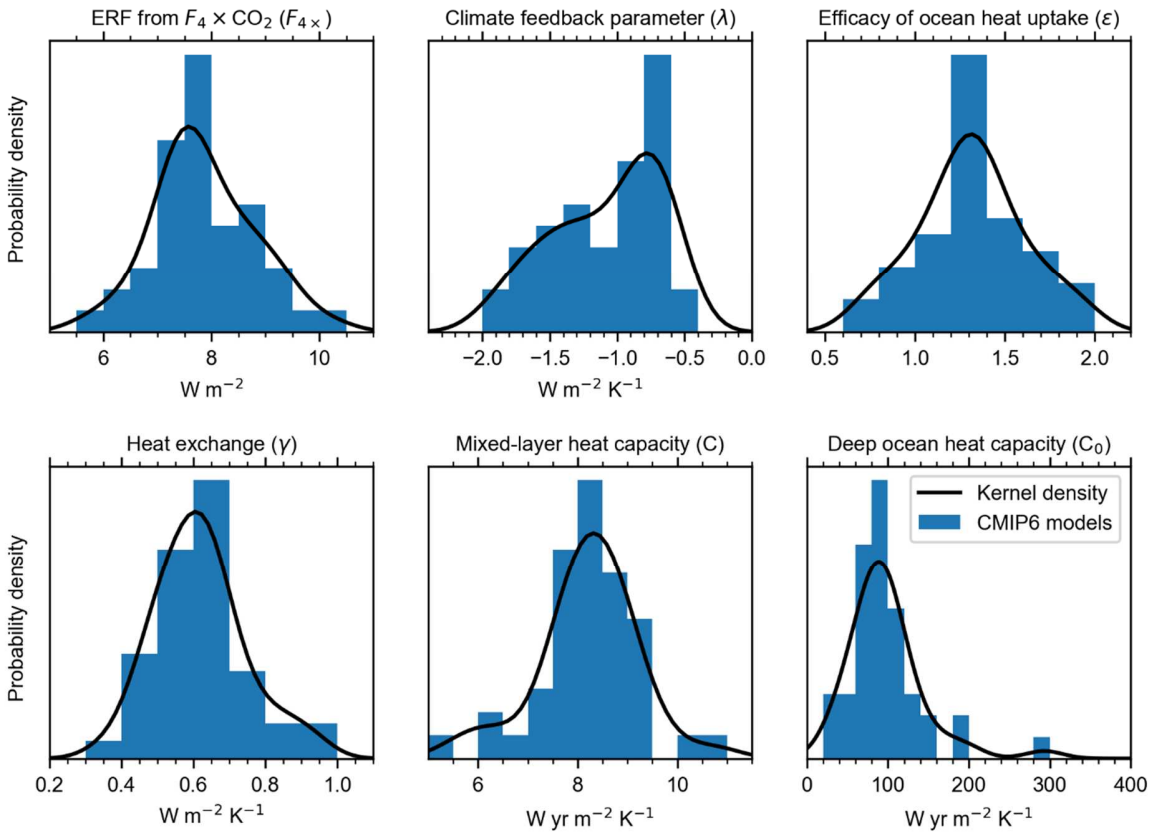

Figure S4: Histograms of Geoffroy model parameter emulations from CMIP6 model and kernel density estimate fit to distributions

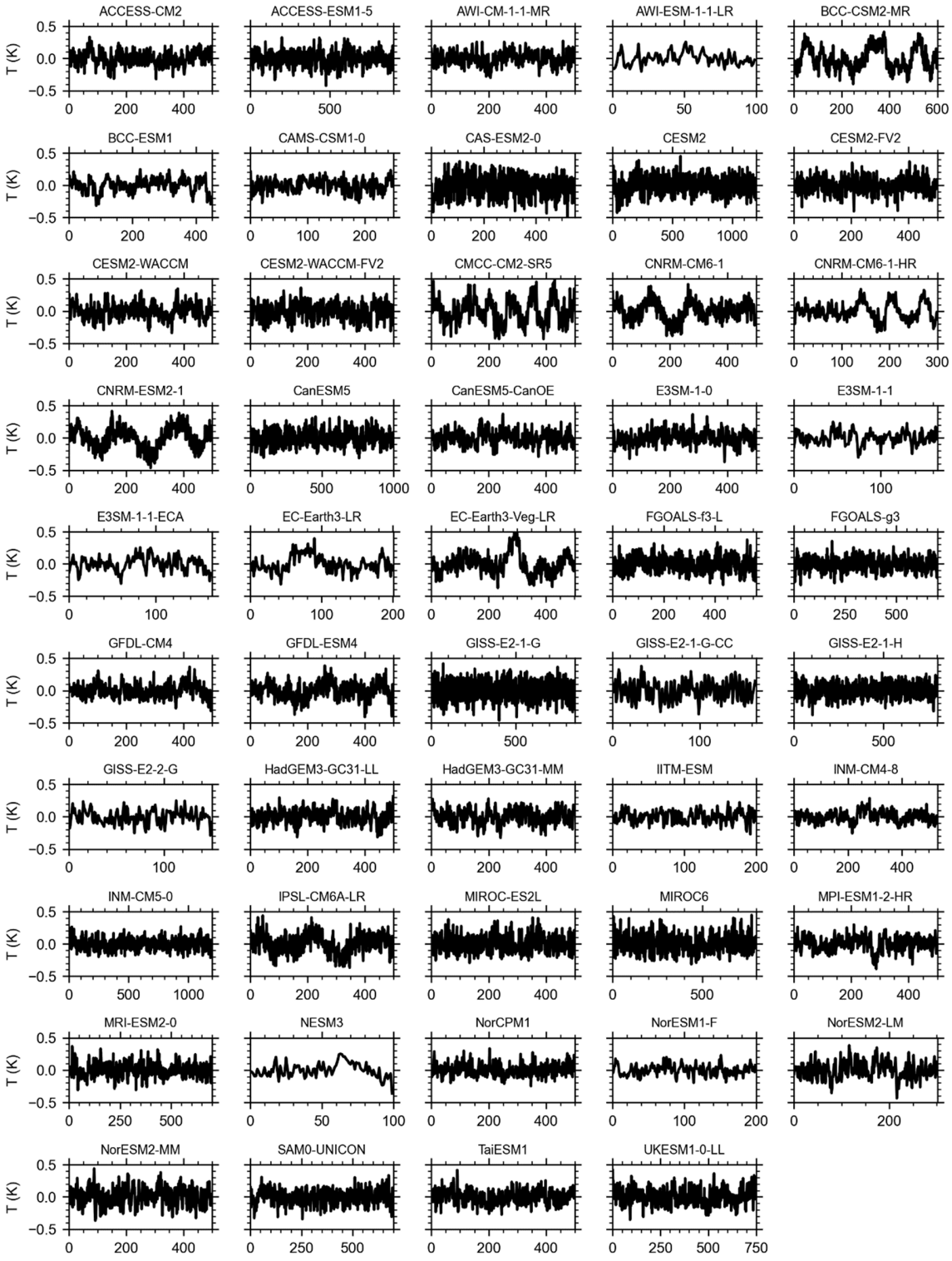

Figure S5: De-trended CMIP6 pre-industrial control global mean temperature anomalies used for characterisation of internal variability.

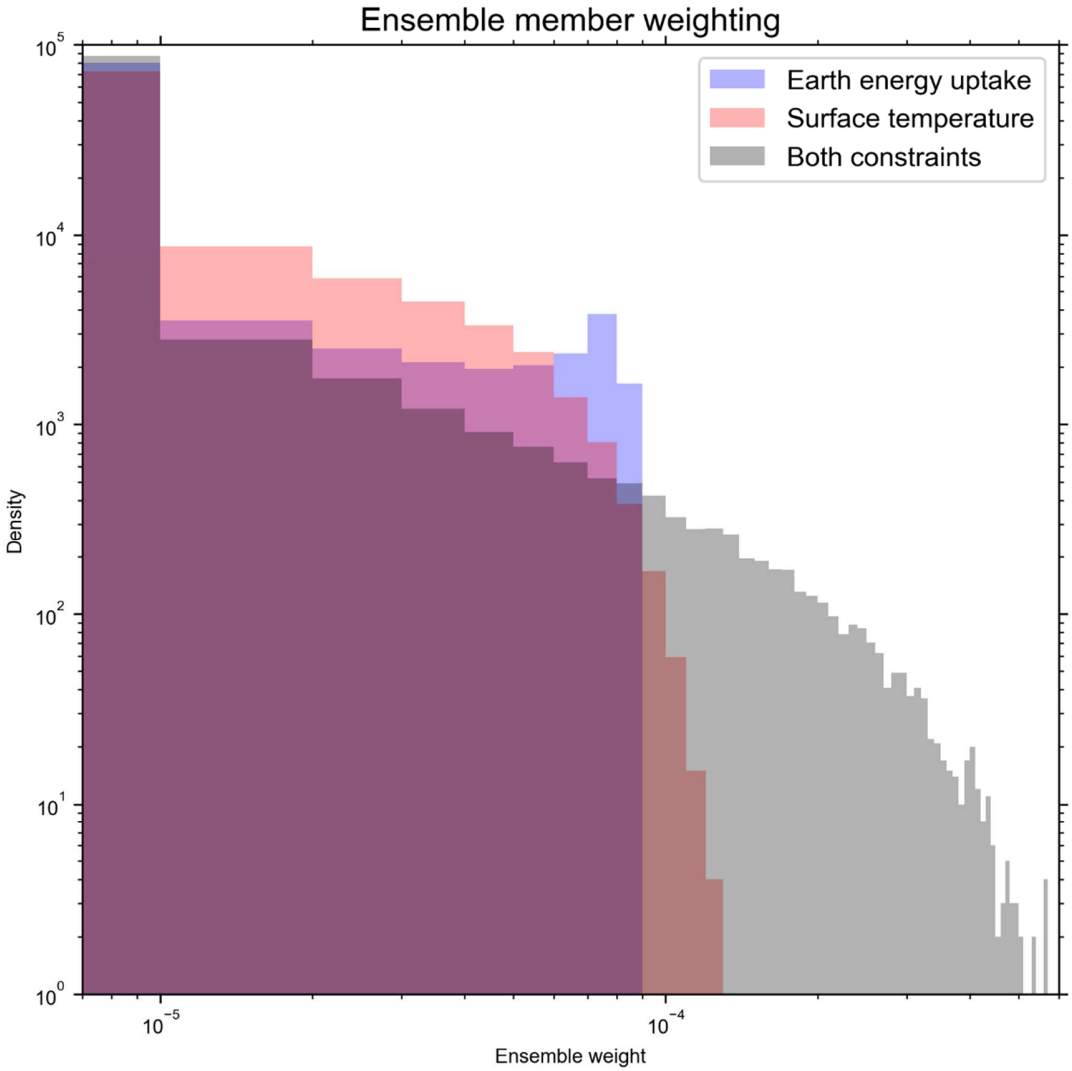

Figure S6: log-log histogram of ensemble member density using ocean heat uptake only (blue), surface temperature only (red) and both constraints (grey). Most ensemble members have a low weight and near-zero contribution to the total ensemble.

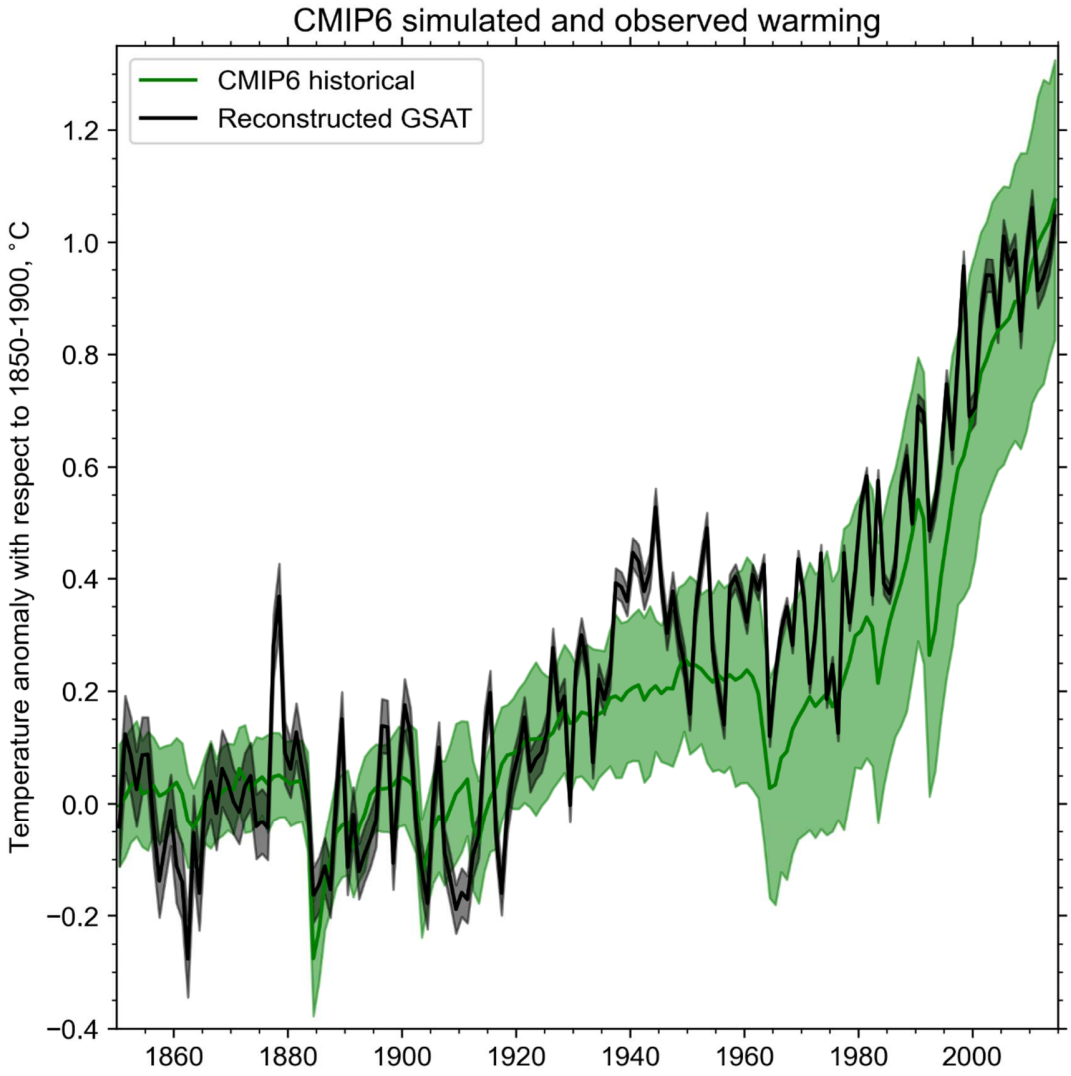

Figure S7: Historical warming simulated by 56 CMIP6 models compared with reconstructed GSAT observations. Anomalies expressed relative to 1850-1900. Models with multiple ensemble members are averaged, and each model contributed equal weight.

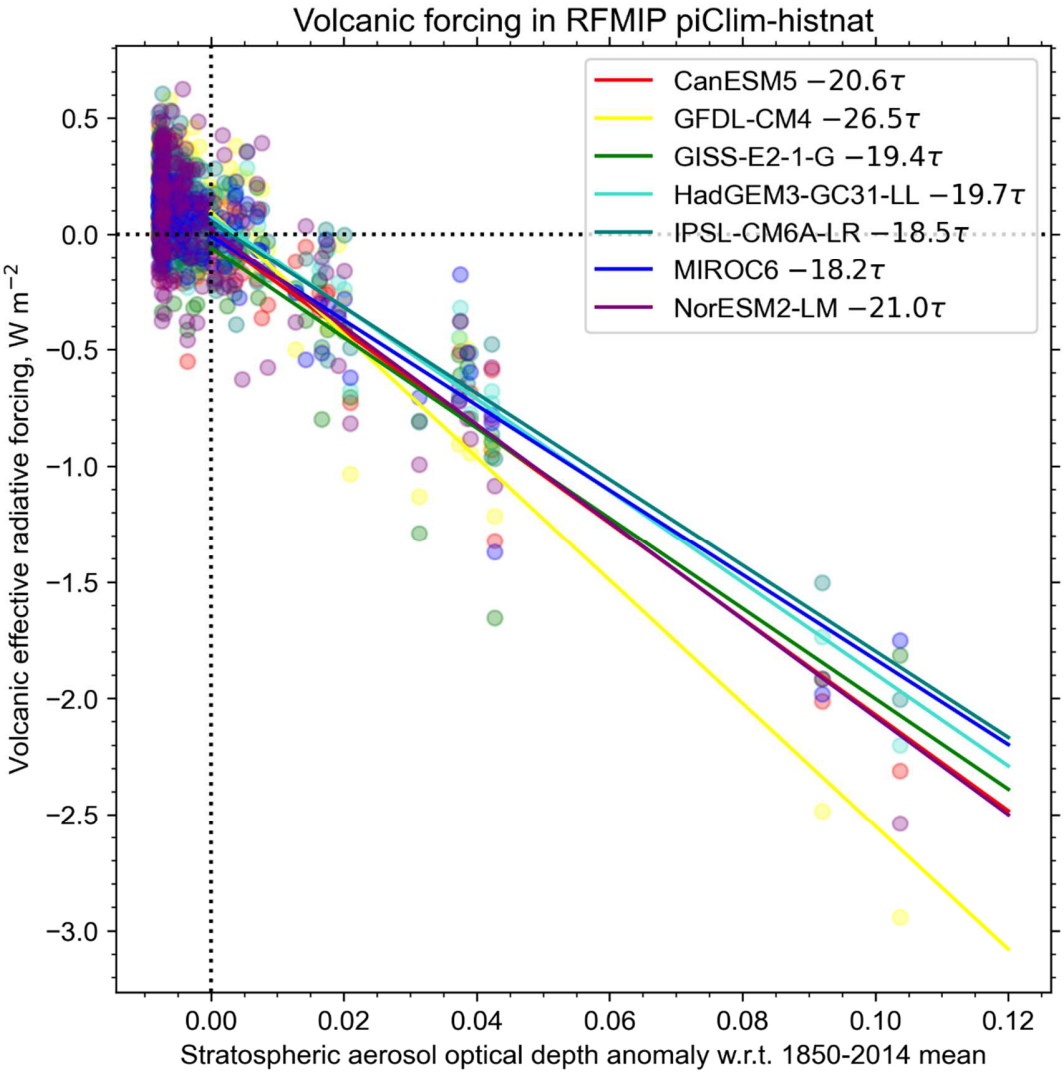

Figure S8: Regression plot of estimate of volcanic forcing from CMIP6 models (RFMIP histnat experiment minus time-varying best estimate of solar forcing, calculated as described in Text S1) against stratospheric aerosol optical depth.

Table S1: Two-layer model parameter fits for CMIP6 models.

Model	**F_{4x}**	**λ**	**C_{mix}**	**C_{deep}**	**γ**	**ε**	**ECS**
ACCESS-CM2	7.66	-0.69	8.82	97.46	0.53	1.49	5.57
ACCESS-ESM1-5	6.97	-0.72	9.02	96.79	0.61	1.71	4.83
AWI-CM-1-1-MR	8.41	-1.30	8.17	54.70	0.49	1.30	3.24
BCC-CSM2-MR	6.89	-1.06	8.51	73.69	0.64	1.32	3.25
BCC-ESM1	6.68	-0.94	8.47	91.72	0.58	1.33	3.57
CAMS-CSM1-0	8.88	-1.88	10.01	62.41	0.53	1.34	2.37
CAS-ESM2-0	7.13	-0.93	7.57	72.83	0.45	1.43	3.84
CESM2	8.84	-0.72	8.33	70.64	0.64	1.73	6.15

Model	F_{4x}	λ	C_{mix}	C_{deep}	γ	ε	ECS
CESM2-FV2	7.94	-0.56	7.96	91.10	0.70	1.91	7.10
CESM2-WACCM	8.28	-0.73	8.72	84.86	0.72	1.63	5.64
CESM2-WACCM-FV2	7.13	-0.59	7.60	111.71	0.71	1.54	6.00
CIESM	8.94	-0.72	8.59	73.23	0.67	1.38	6.25
CNRM-CM6-1	7.51	-0.77	7.05	121.14	0.56	1.03	4.88
CNRM-CM6-1-HR	7.53	-0.94	8.07	90.43	0.58	0.75	3.99
CNRM-ESM2-1	5.70	-0.63	7.48	94.94	0.61	0.87	4.51
CanESM5	7.61	-0.66	7.86	78.83	0.54	1.09	5.78
E3SM-1-0	7.42	-0.64	8.43	43.77	0.36	1.41	5.81
EC-Earth3	7.37	-0.82	8.46	38.41	0.48	1.43	4.48
EC-Earth3-Veg	7.81	-0.85	8.12	38.54	0.45	1.42	4.57
FGOALS-f3-L	9.54	-1.43	9.29	87.98	0.53	1.63	3.33
FGOALS-g3	7.87	-1.28	8.21	112.65	0.67	1.30	3.07
GFDL-CM4	8.45	-0.89	7.36	96.54	0.58	1.85	4.75
GFDL-ESM4	7.34	-1.27	8.44	129.94	0.60	1.23	2.88
GISS-E2-1-G	8.11	-1.46	6.52	145.03	0.85	1.09	2.78
GISS-E2-1-H	7.58	-1.17	8.76	83.36	0.63	1.21	3.25
GISS-E2-2-G	7.25	-1.63	8.63	293.05	0.57	0.72	2.23
HadGEM3-GC31-LL	7.46	-0.62	8.07	78.11	0.51	1.23	5.98
HadGEM3-GC31-MM	7.37	-0.67	7.85	70.75	0.61	1.07	5.53
IITM-ESM	9.25	-1.93	9.38	159.19	0.73	1.07	2.39
INM-CM4-8	6.25	-1.69	7.84	29.20	0.64	1.21	1.85
INM-CM5-0	6.35	-1.59	9.20	51.95	0.55	1.38	2.00
IPSL-CM6A-LR	7.52	-0.76	8.21	60.03	0.44	1.35	4.93
MCM-UA-1-0	7.12	-1.04	8.48	129.93	0.74	0.80	3.41
MIROC-ES2L	7.98	-1.54	10.82	199.60	0.66	0.89	2.59
MIROC6	7.73	-1.36	9.00	182.38	0.64	1.31	2.84
MPI-ESM1-2-HR	8.63	-1.34	8.89	84.13	0.66	1.49	3.23
MPI-ESM1-2-LR	9.28	-1.46	9.25	104.63	0.63	1.29	3.18
MRI-ESM2-0	8.03	-1.20	7.89	92.84	0.94	1.34	3.34
NESM3	7.72	-0.83	5.50	103.69	0.47	0.97	4.62
NorESM2-LM	10.21	-1.77	6.01	115.66	0.90	1.92	2.89
NorESM2-MM	9.39	-1.69	6.13	116.97	0.79	1.66	2.77
SAM0-UNICON	8.69	-1.14	7.67	106.86	0.82	1.21	3.83
TaiESM1	8.51	-0.92	8.72	97.26	0.63	1.27	4.64
UKESM1-0-LL	7.61	-0.68	7.77	77.15	0.54	1.14	5.57

Table S2: Correlation coefficients used for six-dimensional joint kernel density estimate for obtaining random "meta-models" derived from CMIP6 model fits.

	F_{4x}	λ	C	C_0	γ	ε
F_{4x}	1.0000	-0.4649	0.0134	0.0533	0.3159	0.4487
λ		1.0000	-0.3400	-0.3828	-0.1569	0.1990
C			1.0000	0.1686	-0.4411	-0.4355
C_0				1.0000	0.1046	-0.2542
γ					1.0000	0.2857
ε						1.0000

Table S3: 5th, 50th and 95th percentile aerosol forcing trend from 1980-2014 in CMIP6-constrained and 12 CMIP6/chemistry-transport models, in W m^{-2} $decade^{-1}$. Values plotted in Fig. 7.

Time series	5%	mean	95%
CMIP6-constrained	-0.074	0.025	0.111
Unconstrained	-0.086	0.088	0.282
CanESM5	0.042	0.065	0.089
E3SM-1-0	0.020	0.069	0.118
GFDL-CM4	0.040	0.078	0.115
GFDL-ESM4	-0.023	0.037	0.097
GISS-E2-1-G	-0.070	-0.026	0.018
HadGEM3-GC31-LL	0.037	0.066	0.094
IPSL-CM6A-LR	-0.078	-0.03	0.019
MIROC6	-0.040	-0.011	0.017
MRI-ESM2-0	-0.103	-0.024	0.056
NorESM2-LM	0.014	0.064	0.113
UKESM1-0-LL	0.081	0.152	0.222

Table S4: Mean, median, 68% and 90% ranges for aerosol forcing, ECS and TCR from each scaled historical aerosol time series based on weighted percentiles of the distribution after applying constraints. Aerosol ERFs are for 2019 relative to 1750. For CMIP6-constrained, aerosol forcing estimates are from the updated CEDS emissions (O'Rourke et al., 2020), whereas for CMIP6 model estimates they are from SSP2-4.5.

Time series	Variable	5%	16%	median	mean	84%	95%
CMIP6-constrained	ECS (°C)	1.76	2.15	2.89	3.10	3.94	5.11
	TCR (°C)	1.24	1.43	1.80	1.83	2.22	2.57
	ERFaer (W m^{-2})	-1.55	-1.26	-0.87	-0.90	-0.54	-0.35
	ERFari (W m^{-2})	-0.62	-0.47	-0.29	-0.31	-0.15	-0.08
	ERFaci (W m^{-2})	-1.18	-0.93	-0.56	-0.59	-0.26	-0.10
CanESM5	ECS (°C)	1.66	1.98	2.65	2.78	3.44	4.29
	TCR (°C)	1.17	1.34	1.67	1.69	2.03	2.32
	ERFaer (W m^{-2})	-0.97	-0.72	-0.36	-0.39	-0.08	0.08
	ERFari (W m^{-2})	0.04	0.07	0.12	0.12	0.18	0.22
	ERFaci (W m^{-2})	-1.05	-0.83	-0.48	-0.51	-0.22	-0.09
E3SM1-0	ECS (°C)	1.81	2.21	2.95	3.18	4.07	5.32

Time series	Variable	5%	16%	median	mean	84%	95%
	TCR (°C)	1.26	1.47	1.81	1.86	2.24	2.59
	ERFaer (W m^{-2})	-1.28	-1.10	-0.83	-0.83	-0.56	-0.40
	ERFari (W m^{-2})	-0.60	-0.49	-0.33	-0.34	-0.20	-0.13
	ERFaci (W m^{-2})	-0.91	-0.74	-0.48	-0.49	-0.24	-0.10
GFDL-CM4	ECS (°C)	1.75	2.13	2.85	3.03	3.80	4.88
	TCR (°C)	1.23	1.42	1.76	1.79	2.15	2.46
	ERFaer (W m^{-2})	-1.08	-0.88	-0.58	-0.60	-0.33	-0.20
	ERFari (W m^{-2})	-0.21	-0.17	-0.12	-0.12	-0.07	-0.04
	ERFaci (W m^{-2})	-0.98	-0.77	-0.45	-0.48	-0.20	-0.06
GFDL-ESM4	ECS (°C)	1.78	2.17	2.88	3.10	3.91	5.15
	TCR (°C)	1.25	1.44	1.77	1.80	2.16	2.49
	ERFaer (W m^{-2})	-1.23	-1.04	-0.73	-0.74	-0.45	-0.30
	ERFari (W m^{-2})	-0.33	-0.27	-0.18	-0.19	-0.11	-0.07
	ERFaci (W m^{-2})	-1.06	-0.86	-0.54	-0.56	-0.26	-0.11
GISS-E2-1-G	ECS (°C)	1.85	2.29	3.09	3.40	4.41	5.95
	TCR (°C)	1.29	1.50	1.87	1.93	2.35	2.75
	ERFaer (W m^{-2})	-1.70	-1.43	-0.99	-1.00	-0.58	-0.35
	ERFari (W m^{-2})	-0.26	-0.21	-0.15	-0.15	-0.09	-0.06
	ERFaci (W m^{-2})	-1.57	-1.29	-0.84	-0.85	-0.43	-0.20
HadGEM3-GC31-LL	ECS (°C)	1.75	2.13	2.87	3.05	3.86	4.89
	TCR (°C)	1.23	1.42	1.77	1.81	2.18	2.50
	ERFaer (W m^{-2})	-1.36	-1.14	-0.80	-0.81	-0.49	-0.31
	ERFari (W m^{-2})	-0.37	-0.30	-0.20	-0.21	-0.12	-0.08
	ERFaci (W m^{-2})	-1.17	-0.94	-0.58	-0.60	-0.27	-0.10
IPSL-CM6A-LR	ECS (°C)	1.80	2.22	2.98	3.21	4.14	5.42
	TCR (°C)	1.26	1.46	1.83	1.87	2.26	2.63
	ERFaer (W m^{-2})	-1.25	-1.08	-0.82	-0.82	-0.55	-0.40
	ERFari (W m^{-2})	-0.63	-0.51	-0.35	-0.36	-0.21	-0.13
	ERFaci (W m^{-2})	-0.85	-0.70	-0.45	-0.46	-0.23	-0.10
MIROC6	ECS (°C)	1.88	2.32	3.11	3.44	4.46	6.03
	TCR (°C)	1.30	1.52	1.88	1.94	2.36	2.76
	ERFaer (W m^{-2})	-1.62	-1.38	-0.99	-1.00	-0.61	-0.40
	ERFari (W m^{-2})	-0.43	-0.35	-0.24	-0.25	-0.14	-0.09
	ERFaci (W m^{-2})	-1.40	-1.14	-0.73	-0.75	-0.36	-0.16
MRI-ESM2-0	ECS (°C)	1.77	2.16	2.93	3.14	4.00	5.18
	TCR (°C)	1.24	1.44	1.80	1.84	2.23	2.58
	ERFaer (W m^{-2})	-1.27	-1.09	-0.79	-0.80	-0.52	-0.36
	ERFari (W m^{-2})	-0.52	-0.42	-0.29	-0.30	-0.17	-0.11
	ERFaci (W m^{-2})	-0.97	-0.78	-0.49	-0.50	-0.23	-0.10
NorESM2-LM	ECS (°C)	1.76	2.15	2.89	3.09	3.92	5.07
	TCR (°C)	1.24	1.43	1.78	1.82	2.20	2.52
	ERFaer (W m^{-2})	-0.87	-0.67	-0.37	-0.39	-0.12	0.02
	ERFari (W m^{-2})	0.03	0.04	0.07	0.07	0.10	0.13
	ERFaci (W m^{-2})	-0.92	-0.74	-0.44	-0.46	-0.20	-0.07

Time series	Variable	5%	16%	median	mean	84%	95%
Oslo-CTM3	ECS (°C)	1.80	2.22	3.00	3.26	4.17	5.59
	TCR (°C)	1.26	1.47	1.83	1.88	2.28	2.65
	ERFaer (W m^{-2})	-1.42	-1.19	-0.83	-0.86	-0.52	-0.35
	ERFari (W m^{-2})	-0.43	-0.35	-0.24	-0.25	-0.15	-0.09
	ERFaci (W m^{-2})	-1.20	-0.95	-0.58	-0.61	-0.27	-0.10
UKESM1-0-LL	ECS (°C)	1.71	2.07	2.76	2.89	3.62	4.49
	TCR (°C)	1.21	1.39	1.73	1.75	2.10	2.39
	ERFaer (W m^{-2})	-1.13	-0.96	-0.70	-0.71	-0.45	-0.31
	ERFari (W m^{-2})	-0.47	-0.38	-0.26	-0.26	-0.15	-0.10
	ERFaci (W m^{-2})	-0.86	-0.69	-0.42	-0.44	-0.20	-0.07

Table S5: As Table S4, using only global-mean surface air temperature as the constraint.

Time series	Variable	5%	16%	median	mean	84%	95%
CMIP6-constrained	ECS (°C)	1.93	2.34	3.08	3.39	4.36	5.84
	TCR (°C)	1.33	1.53	1.84	1.89	2.25	2.60
	ERFaer (W m^{-2})	-1.43	-1.14	-0.77	-0.80	-0.45	-0.28
	ERFari (W m^{-2})	-0.59	-0.44	-0.27	-0.29	-0.13	-0.06
	ERFaci (W m^{-2})	-1.08	-0.82	-0.48	-0.51	-0.21	-0.05
CanESM5	ECS (°C)	1.89	2.29	2.96	3.22	4.06	5.35
	TCR (°C)	1.31	1.50	1.79	1.82	2.15	2.44
	ERFaer (W m^{-2})	-0.83	-0.59	-0.25	-0.29	0.00	0.14
	ERFari (W m^{-2})	0.05	0.07	0.13	0.13	0.18	0.22
	ERFaci (W m^{-2})	-0.93	-0.70	-0.38	-0.42	-0.15	-0.02
E3SM1-0	ECS (°C)	1.92	2.33	3.06	3.38	4.33	5.84
	TCR (°C)	1.33	1.53	1.84	1.89	2.25	2.60
	ERFaer (W m^{-2})	-1.22	-1.04	-0.76	-0.77	-0.49	-0.34
	ERFari (W m^{-2})	-0.57	-0.46	-0.31	-0.33	-0.19	-0.12
	ERFaci (W m^{-2})	-0.87	-0.69	-0.43	-0.44	-0.19	-0.07
GFDL-CM4	ECS (°C)	1.92	2.33	3.04	3.33	4.26	5.65
	TCR (°C)	1.33	1.53	1.82	1.87	2.21	2.52
	ERFaer (W m^{-2})	-1.01	-0.80	-0.52	-0.54	-0.28	-0.15
	ERFari (W m^{-2})	-0.20	-0.16	-0.11	-0.12	-0.07	-0.04
	ERFaci (W m^{-2})	-0.91	-0.69	-0.40	-0.42	-0.15	-0.02
GFDL-ESM4	ECS (°C)	1.89	2.28	2.96	3.22	4.07	5.41
	TCR (°C)	1.31	1.50	1.79	1.83	2.16	2.47
	ERFaer (W m^{-2})	-1.17	-0.96	-0.64	-0.66	-0.38	-0.23
	ERFari (W m^{-2})	-0.32	-0.26	-0.18	-0.18	-0.10	-0.07
	ERFaci (W m^{-2})	-1.00	-0.78	-0.45	-0.48	-0.19	-0.06
GISS-E2-1-G	ECS (°C)	1.95	2.37	3.15	3.51	4.56	6.24
	TCR (°C)	1.34	1.55	1.88	1.94	2.33	2.72
	ERFaer (W m^{-2})	-1.62	-1.32	-0.87	-0.89	-0.47	-0.26
	ERFari (W m^{-2})	-0.26	-0.21	-0.14	-0.15	-0.08	-0.05
	ERFaci (W m^{-2})	-1.49	-1.18	-0.72	-0.75	-0.32	-0.12
HadGEM3-	ECS (°C)	1.93	2.34	3.07	3.37	4.32	5.78

Time series	Variable	5%	16%	median	mean	84%	95%
GC31-LL	TCR (°C)	1.33	1.53	1.84	1.88	2.24	2.57
	ERFaer (W m^{-2})	-1.29	-1.07	-0.73	-0.75	-0.43	-0.27
	ERFari (W m^{-2})	-0.36	-0.29	-0.20	-0.20	-0.12	-0.07
	ERFaci (W m^{-2})	-1.10	-0.87	-0.52	-0.55	-0.23	-0.06
IPSL-CM6A-LR	ECS (°C)	1.94	2.35	3.12	3.45	4.46	6.04
	TCR (°C)	1.34	1.54	1.86	1.92	2.30	2.67
	ERFaer (W m^{-2})	-1.20	-1.03	-0.76	-0.76	-0.50	-0.35
	ERFari (W m^{-2})	-0.60	-0.48	-0.32	-0.34	-0.19	-0.12
	ERFaci (W m^{-2})	-0.81	-0.66	-0.41	-0.42	-0.20	-0.08
MIROC6	ECS (°C)	1.95	2.38	3.17	3.53	4.58	6.27
	TCR (°C)	1.35	1.56	1.88	1.94	2.34	2.72
	ERFaer (W m^{-2})	-1.56	-1.29	-0.88	-0.90	-0.52	-0.32
	ERFari (W m^{-2})	-0.42	-0.34	-0.23	-0.24	-0.14	-0.09
	ERFaci (W m^{-2})	-1.34	-1.05	-0.63	-0.66	-0.28	-0.09
MRI-ESM2-0	ECS (°C)	1.93	2.34	3.08	3.39	4.35	5.82
	TCR (°C)	1.33	1.54	1.85	1.89	2.25	2.60
	ERFaer (W m^{-2})	-1.20	-1.01	-0.71	-0.73	-0.45	-0.31
	ERFari (W m^{-2})	-0.51	-0.41	-0.28	-0.29	-0.17	-0.11
	ERFaci (W m^{-2})	-0.90	-0.70	-0.42	-0.44	-0.18	-0.06
NorESM2-LM	ECS (°C)	1.93	2.34	3.07	3.38	4.33	5.79
	TCR (°C)	1.33	1.53	1.84	1.88	2.24	2.57
	ERFaer (W m^{-2})	-0.79	-0.59	-0.31	-0.33	-0.08	0.05
	ERFari (W m^{-2})	0.03	0.04	0.07	0.07	0.10	0.13
	ERFaci (W m^{-2})	-0.85	-0.66	-0.38	-0.40	-0.16	-0.03
Oslo-CTM3	ECS (°C)	1.95	2.37	3.15	3.49	4.51	6.13
	TCR (°C)	1.34	1.55	1.87	1.92	2.30	2.66
	ERFaer (W m^{-2})	-1.34	-1.09	-0.74	-0.77	-0.45	-0.29
	ERFari (W m^{-2})	-0.43	-0.35	-0.24	-0.25	-0.14	-0.09
	ERFaci (W m^{-2})	-1.11	-0.86	-0.49	-0.52	-0.20	-0.05
UKESM1-0-LL	ECS (°C)	1.90	2.31	3.00	3.27	4.15	5.47
	TCR (°C)	1.32	1.52	1.81	1.85	2.18	2.49
	ERFaer (W m^{-2})	-1.07	-0.91	-0.65	-0.66	-0.41	-0.28
	ERFari (W m^{-2})	-0.44	-0.36	-0.24	-0.25	-0.14	-0.09
	ERFaci (W m^{-2})	-0.82	-0.65	-0.39	-0.41	-0.17	-0.05

Table S6: As Table S4, using only Earth energy uptake as the constraint.

Time series	Variable	5%	16%	median	mean	84%	95%
CMIP6-constrained	ECS (°C)	1.95	2.38	3.26	3.75	4.98	7.12
	TCR (°C)	1.33	1.54	1.94	2.05	2.55	3.13
	ERFaer (W m^{-2})	-1.83	-1.53	-1.09	-1.10	-0.66	-0.39
	ERFari (W m^{-2})	-0.64	-0.47	-0.29	-0.30	-0.14	-0.02
	ERFaci (W m^{-2})	-1.48	-1.20	-0.78	-0.80	-0.39	-0.18
CanESM5	ECS (°C)	1.90	2.33	3.20	3.68	4.89	7.00

Time series	Variable	5%	16%	median	mean	84%	95%
	TCR (°C)	1.31	1.52	1.91	2.02	2.51	3.09
	ERFaer (W m^{-2})	-1.22	-0.96	-0.56	-0.57	-0.18	0.04
	ERFari (W m^{-2})	0.08	0.13	0.21	0.21	0.30	0.36
	ERFaci (W m^{-2})	-1.40	-1.15	-0.77	-0.78	-0.40	-0.20
E3SM1-0	ECS (°C)	1.96	2.38	3.25	3.73	4.95	7.03
	TCR (°C)	1.33	1.54	1.94	2.04	2.54	3.11
	ERFaer (W m^{-2})	-1.52	-1.32	-0.99	-0.99	-0.65	-0.46
	ERFari (W m^{-2})	-0.63	-0.52	-0.36	-0.37	-0.22	-0.14
	ERFaci (W m^{-2})	-1.15	-0.94	-0.62	-0.62	-0.30	-0.14
GFDL-CM4	ECS (°C)	1.99	2.41	3.30	3.80	5.10	7.23
	TCR (°C)	1.35	1.56	1.95	2.07	2.57	3.16
	ERFaer (W m^{-2})	-1.40	-1.18	-0.83	-0.84	-0.49	-0.30
	ERFari (W m^{-2})	-0.25	-0.21	-0.14	-0.15	-0.09	-0.06
	ERFaci (W m^{-2})	-1.27	-1.04	-0.67	-0.69	-0.33	-0.15
GFDL-ESM4	ECS (°C)	1.96	2.39	3.27	3.76	5.01	7.13
	TCR (°C)	1.33	1.54	1.94	2.05	2.55	3.14
	ERFaer (W m^{-2})	-1.46	-1.26	-0.93	-0.92	-0.58	-0.39
	ERFari (W m^{-2})	-0.41	-0.33	-0.23	-0.24	-0.14	-0.09
	ERFaci (W m^{-2})	-1.23	-1.02	-0.68	-0.69	-0.35	-0.17
GISS-E2-1-G	ECS (°C)	1.97	2.39	3.26	3.75	4.98	7.09
	TCR (°C)	1.33	1.54	1.94	2.05	2.55	3.13
	ERFaer (W m^{-2})	-1.93	-1.62	-1.14	-1.14	-0.65	-0.39
	ERFari (W m^{-2})	-0.27	-0.22	-0.15	-0.16	-0.09	-0.06
	ERFaci (W m^{-2})	-1.78	-1.47	-0.98	-0.98	-0.49	-0.24
HadGEM3-GC31-LL	ECS (°C)	1.96	2.38	3.27	3.75	4.98	7.07
	TCR (°C)	1.33	1.54	1.94	2.05	2.55	3.12
	ERFaer (W m^{-2})	-1.85	-1.57	-1.13	-1.13	-0.68	-0.43
	ERFari (W m^{-2})	-0.41	-0.33	-0.23	-0.24	-0.14	-0.09
	ERFaci (W m^{-2})	-1.63	-1.34	-0.89	-0.89	-0.44	-0.20
IPSL-CM6A-LR	ECS (°C)	1.97	2.39	3.27	3.75	4.99	7.07
	TCR (°C)	1.34	1.54	1.94	2.05	2.55	3.13
	ERFaer (W m^{-2})	-1.54	-1.34	-1.01	-1.00	-0.66	-0.46
	ERFari (W m^{-2})	-0.62	-0.51	-0.35	-0.36	-0.21	-0.14
	ERFaci (W m^{-2})	-1.16	-0.96	-0.64	-0.64	-0.32	-0.15
MIROC6	ECS (°C)	1.98	2.41	3.29	3.78	5.03	7.13
	TCR (°C)	1.34	1.55	1.95	2.06	2.56	3.14
	ERFaer (W m^{-2})	-1.81	-1.54	-1.11	-1.11	-0.68	-0.44
	ERFari (W m^{-2})	-0.45	-0.37	-0.25	-0.26	-0.15	-0.10
	ERFaci (W m^{-2})	-1.56	-1.28	-0.84	-0.85	-0.41	-0.19
MRI-ESM2-0	ECS (°C)	1.93	2.35	3.19	3.66	4.86	6.93
	TCR (°C)	1.32	1.52	1.92	2.03	2.53	3.10
	ERFaer (W m^{-2})	-1.56	-1.36	-1.00	-1.00	-0.63	-0.42
	ERFari (W m^{-2})	-0.54	-0.45	-0.31	-0.32	-0.19	-0.12
	ERFaci (W m^{-2})	-1.24	-1.02	-0.67	-0.68	-0.32	-0.15

Time series	Variable	5%	16%	median	mean	84%	95%
NorESM2-LM	ECS (°C)	1.97	2.39	3.28	3.76	5.01	7.11
	TCR (°C)	1.34	1.55	1.94	2.05	2.56	3.13
	ERFaer (W m^{-2})	-1.10	-0.89	-0.55	-0.56	-0.22	-0.05
	ERFari (W m^{-2})	0.03	0.05	0.08	0.09	0.12	0.15
	ERFaci (W m^{-2})	-1.18	-0.97	-0.63	-0.64	-0.31	-0.14
Oslo-CTM3	ECS (°C)	1.97	2.39	3.28	3.77	5.02	7.14
	TCR (°C)	1.34	1.55	1.94	2.05	2.56	3.13
	ERFaer (W m^{-2})	-1.68	-1.43	-1.04	-1.04	-0.65	-0.43
	ERFari (W m^{-2})	-0.50	-0.41	-0.28	-0.29	-0.17	-0.11
	ERFaci (W m^{-2})	-1.40	-1.14	-0.74	-0.75	-0.36	-0.16
UKESM1-0-LL	ECS (°C)	1.93	2.35	3.23	3.70	4.90	6.97
	TCR (°C)	1.32	1.53	1.93	2.03	2.53	3.10
	ERFaer (W m^{-2})	-1.63	-1.40	-1.03	-1.03	-0.65	-0.43
	ERFari (W m^{-2})	-0.50	-0.41	-0.29	-0.29	-0.18	-0.11
	ERFaci (W m^{-2})	-1.35	-1.11	-0.73	-0.73	-0.35	-0.16

References

Bond, T. C., Doherty, S. J., Fahey, D. W., Forster, P. M., Berntsen, T., Deangelo, B. J., et al. (2013). Bounding the role of black carbon in the climate system: A scientific assessment. *Journal of Geophysical Research Atmospheres*, *118*(11), 5380–5552. https://doi.org/10.1002/jgrd.50171

Etminan, M., Myhre, G., Highwood, E. J., & Shine, K. P. (2016). Radiative forcing of carbon dioxide, methane, and nitrous oxide: A significant revision of the methane radiative forcing. *Geophysical Research Letters*, *43*(24), 12,614-12,623. https://doi.org/10.1002/2016GL071930

Ghimire, B., Williams, C. A., Masek, J., Gao, F., Wang, Z., Schaaf, C., & He, T. (2014). Global albedo change and radiative cooling from anthropogenic land cover change, 1700 to 2005 based on MODIS, land use harmonization, radiative kernels, and reanalysis. *Geophysical Research Letters*, *41*(24), 9087–9096. https://doi.org/10.1002/2014GL061671

Gidden, M. J., Riahi, K., Smith, S. J., Fujimori, S., Luderer, G., Kriegler, E., et al. (2019). Global emissions pathways under different socioeconomic scenarios for use in CMIP6: a dataset of harmonized emissions trajectories through the end of the century. *Geoscientific Model Development*, *12*(4), 1443–1475. https://doi.org/10.5194/gmd-12-1443-2019

Global Volcanism Program. (2013). Volcanoes of the World v.4.9.0. Smithsonian Institution. https://doi.org/10.5479/si.GVP.VOTW4-2013

Gray, L. J., Rumbold, S. T., & Shine, K. P. (2009). Stratospheric Temperature and Radiative Forcing Response to 11-Year Solar Cycle Changes in Irradiance and Ozone. *Journal of the Atmospheric Sciences*, *66*(8), 2402–2417. https://doi.org/10.1175/2009JAS2866.1

Hodnebrog, Ø., Myhre, G., Kramer, R. J., Shine, K. P., Andrews, T., Faluvegi, G., et al. (2020). The effect of rapid adjustments to halocarbons and N2O on radiative

forcing. *Npj Climate and Atmospheric Science*, *3*(1). https://doi.org/10.1038/s41612-020-00150-x

Hodnebrog, Ø., Aamaas, B., Fuglestvedt, J. S., Marston, G., Myhre, G., Nielsen, C. J., et al. (2020). Updated Global Warming Potentials and Radiative Efficiencies of Halocarbons and Other Weak Atmospheric Absorbers. *Reviews of Geophysics*, *58*(3). https://doi.org/10.1029/2019RG000691

Kovilakam, M., Thomason, L. W., Ernest, N., Rieger, L., Bourassa, A., & Millán, L. (2020). The Global Space-based Stratospheric Aerosol Climatology (version 2.0): 1979–2018. *Earth System Science Data*, *12*(4), 2607–2634. https://doi.org/10.5194/essd-12-2607-2020

Larson, E. J. L., & Portmann, R. W. (2016). A temporal kernel method to compute effective radiative forcing in CMIP5 transient simulations. *Journal of Climate*, *29*(4), 1497–1509. https://doi.org/10.1175/JCLI-D-15-0577.1

Lee, D. S., Fahey, D. W., Skowron, A., Allen, M. R., Burkhardt, U., Chen, Q., et al. (2020). The contribution of global aviation to anthropogenic climate forcing for 2000 to 2018. *Atmospheric Environment*, *244*, 117834. https://doi.org/10.1016/j.atmosenv.2020.117834

Matthes, K., Funke, B., Andersson, M. E., Barnard, L., Beer, J., Charbonneau, P., et al. (2017). Solar forcing for CMIP6 (v3.2). *Geoscientific Model Development*, *10*(6), 2247–2302. https://doi.org/10.5194/gmd-10-2247-2017

Meinshausen, M., Vogel, E., Nauels, A., Lorbacher, K., Meinshausen, N., Etheridge, D. M., et al. (2017). Historical greenhouse gas concentrations for climate modelling (CMIP6). *Geoscientific Model Development*, *10*(5), 2057–2116. https://doi.org/10.5194/gmd-10-2057-2017

Meinshausen, M., Nicholls, Z. R. J., Lewis, J., Gidden, M. J., Vogel, E., Freund, M., et al. (2020). The shared socio-economic pathway (SSP) greenhouse gas concentrations and their extensions to 2500. *Geoscientific Model Development*, *13*(8), 3571–3605. https://doi.org/10.5194/gmd-13-3571-2020

Myhre, G., Shindell, D., Bréon, F.-M., Collins, W., Fuglestvedt, J., Huang, J., et al. (2013a). Anthropogenic and natural radiative forcing. In T. F. Stocker, D. Qin, G.-K. Plattner, M. Tignor, S. K. Allen, J. Boschung, et al. (Eds.), *Climate Change 2013 the Physical Science Basis: Working Group I Contribution to the Fifth Assessment Report of the Intergovernmental Panel on Climate Change* (Vol. 9781107057, pp. 659–740). Cambridge, United Kingdom and New York, NY, USA: Cambridge University Press. https://doi.org/10.1017/CBO9781107415324.018

Myhre, G., Shindell, D., Bréon, F.-M., Collins, W., Fuglestvedt, J., Huang, J., et al. (2013b). Anthropogenic and Natural Radiative Forcing. In Intergovernmental Panel on Climate Change (Ed.), *Climate Change 2013 - The Physical Science Basis* (pp. 659–740). Cambridge: Cambridge University Press. https://doi.org/10.1017/CBO9781107415324.018

O'Rourke, P. R., Smith, S. J., McDuffie, E. E., Klimont, Z., Crippa, M., Mott, A., et al. (2020, September). CEDS v_2020_09_11 Pre-Release Emission Data. Zenodo. https://doi.org/10.5281/zenodo.4025316

Sherwood, S., Dixit, V., & Salomez, C. (2018). The global warming potential of near-surface emitted water vapour. *Environmental Research Letters*, *13*(10). https://doi.org/10.1088/1748-9326/aae018

Skeie, R. B., Myhre, G., Hodnebrog, Ø., Cameron-Smith, P. J., Deushi, M., Hegglin, M. I., et al. (2020). Historical total ozone radiative forcing derived from CMIP6 simulations. *Npj Climate and Atmospheric Science*, *3*(1). https://doi.org/10.1038/s41612-020-00131-0

Smith, C. J., Forster, P. M., Allen, M., Leach, N., Millar, R. J., Passerello, G. A., & Regayre, L. A. (2018). FAIR v1.3: a simple emissions-based impulse response and carbon cycle model. *Geoscientific Model Development*, *11*(6), 2273–2297. https://doi.org/10.5194/gmd-11-2273-2018

Smith, C. J., Kramer, R. J., Myhre, G., Forster, P. M., Soden, B. J., Andrews, T., et al. (2018). Understanding Rapid Adjustments to Diverse Forcing Agents. *Geophysical Research Letters*, *45*(21), 12,023-12,031. https://doi.org/10.1029/2018GL079826

Smith, C. J., Kramer, R. J., Myhre, G., Alterskjær, K., Collins, W., Sima, A., et al. (2020). Effective radiative forcing and adjustments in CMIP6 models. *Atmospheric Chemistry and Physics*, *20*(16), 9591–9618. https://doi.org/10.5194/acp-20-9591-2020

Stevenson, D. S., Young, P. J., Naik, V., Lamarque, J.-F., Shindell, D. T., Voulgarakis, A., et al. (2013). Tropospheric ozone changes, radiative forcing and attribution to emissions in the Atmospheric Chemistry and Climate Model Intercomparison Project (ACCMIP). *Atmospheric Chemistry and Physics*, *13*(6), 3063–3085. https://doi.org/10.5194/acp-13-3063-2013

Toohey, M., & Sigl, M. (2017). Volcanic stratospheric sulfur injections and aerosol optical depth from 500 BCE to 1900 CE. *Earth System Science Data*, *9*(2), 809–831. https://doi.org/10.5194/essd-9-809-2017

Vieira, L. E. A., Solanki, S. K., Krivova, N. A., & Usoskin, I. (2011). Evolution of the solar irradiance during the Holocene. *Astronomy & Astrophysics*, *531*, A6. https://doi.org/10.1051/0004-6361/201015843